Fractal Nanoparticle Plasmonics: The Cayley Tree

Samuel Gottheim,[†,‡,⊥] Hui Zhang,[§,⊥] Alexander O. Govorov,[§] and Naomi J. Halas*[,†,‡]

[†]Department of Chemistry and [‡]Laboratory for Nanophotonics, Rice University, Houston, Texas 77005, United States and [§]Department of Physics and Astronomy, Ohio University, Athens, Ohio 45701, United States. [⊥]These authors (S.G. and H.Z.) contributed equally.

ABSTRACT There has been strong, ongoing interest over the past decade in developing strategies to design and engineer materials with tailored optical properties. Fractal-like nanoparticles and films have long been known to possess a remarkably broad-band optical response and are potential nanoscale components for realizing spectrum-spanning optical effects. Here we examine the role of self-similarity in a fractal geometry for the design of plasmon line shapes. By computing and fabricating simple Cayley tree nanostructures of increasing fractal order *N*, we are able to identify the principle behind how the multimodal plasmon spectrum of this system develops as the fractal order is increased. With increasing *N*, the fractal structure acquires an increasing number of modes with certain degeneracies: these modes correspond to plasmon oscillations on the different length scales inside a fractal. As a result, fractals with large *N* exhibit broad, multipeaked spectra from plasmons with large degeneracy numbers. The Cayley tree serves as an example of a more general, fractal-based route for the design of structures and media with highly complex optical line shapes.

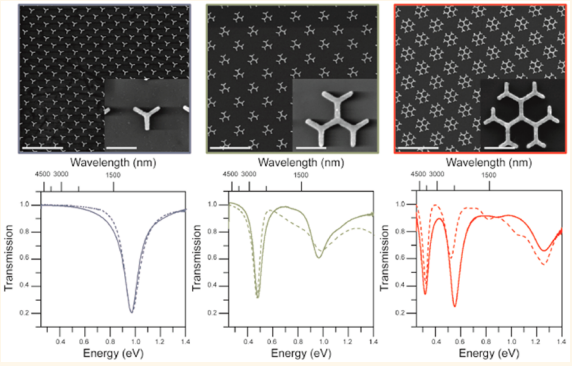

KEYWORDS: plasmons · fractal · Cayley tree · nanoantenna

Metallic nanostructures support surface plasmons, the collective oscillation of conduction band electrons, allowing for the manipulation of light at the nanoscale. The design of plasmonic nanoantennas with engineered line shapes has been of widespread growing interest. This topic has been the driving force behind innovations in chemical-sensing technologies, such as surface-enhanced Raman spectroscopy,[1] surface-enhanced infrared absorption spectroscopy,[2] and other areas such as nonlinear optics.[3] The ability of nanoantennas to concentrate optical energy into subdiffraction volumes, allowing for strong electromagnetic field enhancements, is critical to these advances.

A common aspect of these applications is the ability to engineer and tune optical properties based on metallic structures with specific geometries. In recent decades, strides in top-down fabrication and bottom-up synthesis have allowed for exploration of 2D and 3D geometries, such as nanodisks,[4] spheres,[5] nanoshells,[6] nanomatryushkas,[7] nanoprisms,[8] nanorods,[9] nanobelts,[10] and nanostars.[11] Top-down methods, such as e-beam lithography[12] and hole-mask lithography,[13] allow for precise control of size and geometry for both individual nanoparticles and extended arrays of nanoparticles, while synthetic methods allow for larger-scale production with limited control of size and geometry.

To adapt a successful concept from microwave and radio frequency antenna design,[14] we investigate the plasmonic properties of simple fractal antennas at optical length scales. In macroscopic antennas, it is well-known that self-similarity can give rise to a broad-band (multifrequency) electromagnetic response. Previous work has focused on studies of fractal-like films and clusters,[15−18] the Sierpinski nanocarpet,[19] the Vicsek fractal,[18,20,21] and trapezoidal log-periodic geometries.[3,22] Multiparticle fractal structures have been shown to function as "nanolenses".[23,24] Here, we systematically investigate a simple branching fractal geometry, the Cayley tree, to elucidate the underlying principles that govern the optical response of more complex

* Address correspondence to halas@rice.edu.

Received for review January 19, 2015 and accepted February 28, 2015.

Published online February 28, 2015
10.1021/acsnano.5b00412

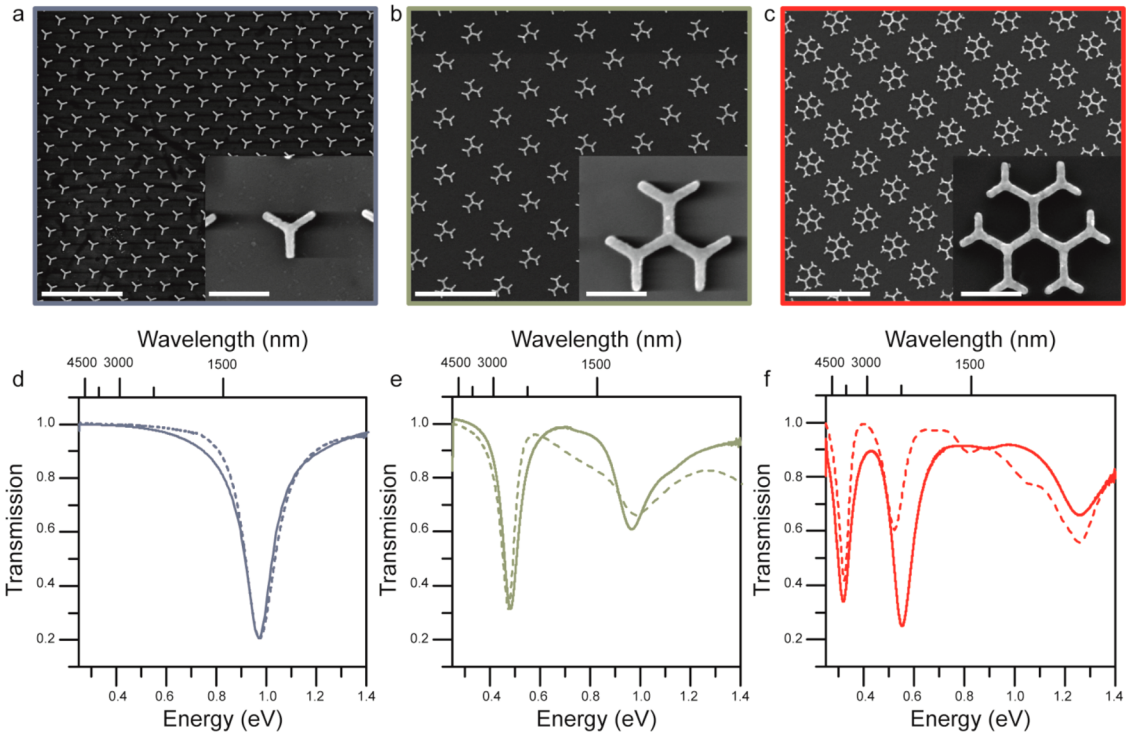

Figure 1. Scanning electron micrograph (SEM) images of 50 × 50 μm 2D arrays of (a) first-, (b) second-, and (c) third-order Cayley trees with the individual structures shown as insets. The periodicity of the first-order Cayley tree (a) is 500 nm in both directions, while the (b) second- and (c) third-order Cayley trees have 1 μm periodicity. The array scale bars are 2 μm; inset scale bars are 300 nm. (d–f) Experimental Fourier transform infrared transmission spectra (solid lines) of the first-, second-, and third-order Cayley tree structures under nonpolarized light excitation with corresponding finite element method simulated transmission spectra (dashed lines) reveal an increase in the number of resonances as the fractal geometry is iterated. Each newly emerging resonance occurs at an energy lower than those seen previously.

fractal nanoparticle geometries. Theoretically, the Cayley tree geometry can be iterated indefinitely, as an area-filling self-similar geometry constructed of arbitrarily long lines. As an experimentally realized structure, however, standard e-beam lithography limits the smallest feature size to approximately 20 nm, so we limit our study to the first three iterations of the Cayley tree structure. Our goal is to provide an additional tool in the engineering of plasmonic optical response by obtaining greater insight into the optical response of fractal-like particles.

RESULTS AND DISCUSSION

Fractal Order. The construction of a Cayley tree is by straightforward iterative function. The geometry is generated from an equilateral Y shape (the first-order fractal, $N = 1$, Figure 1a). Upon each iteration, two new arms are added to each terminal branch. The angle between each branch is kept constant at $\theta = 120°$, maintaining a three-fold rotational symmetry. The arm lengths and symmetry are varied throughout this study to investigate the properties of this structure.

To examine the effect of fractal order on optical response, the first-, second-, and third-order Au Cayley tree structures were fabricated using e-beam lithography, and their optical responses were measured using a commercial Fourier transform infrared (FTIR, Bruker Vertex 80v Hyperion 3000) microscope. The scanning electron micrograph (ESEM, FEI Quanta 600) images of the first-, second-, and third-order Cayley tree structures are shown in Figure 1a–c. The 50 nm thick gold structures were fabricated in 2D arrays on a high-grade quartz substrate with a 2 nm Ti adhesion layer (see Materials and Methods). Arm lengths in the first- and second-order structure were L_1, $L_2 = 140$ nm, while the arm widths were $W = 40$ nm. In the third-order structure, the outermost arm lengths were reduced to $L_3 = 100$ nm to prevent overlap between neighboring structures. The inner arm lengths remained at L_1, $L_2 = 140$ nm, and the width of all arms was $W = 40$ nm. All particles were fabricated in 50 × 50 μm arrays; the first-order structures had a 0.5 μm periodicity, while the second- and third-order structures were fabricated with 1 μm periodicity. No coupling between the near fields of adjacent particles was observed at these distances. The optical properties were characterized by FTIR using nonpolarized incident light (NA = 0.5). All measurements were performed by placing a 40 × 40 μm^2 aperture coincident with the center of the array. To obtain theoretical predictions of the optical response of these structures, the geometries were simulated using the finite element method (FEM, COMSOL Multiphysics).[25]

The experimental transmission spectra (solid lines) and simulated spectra (dashed lines) are plotted in

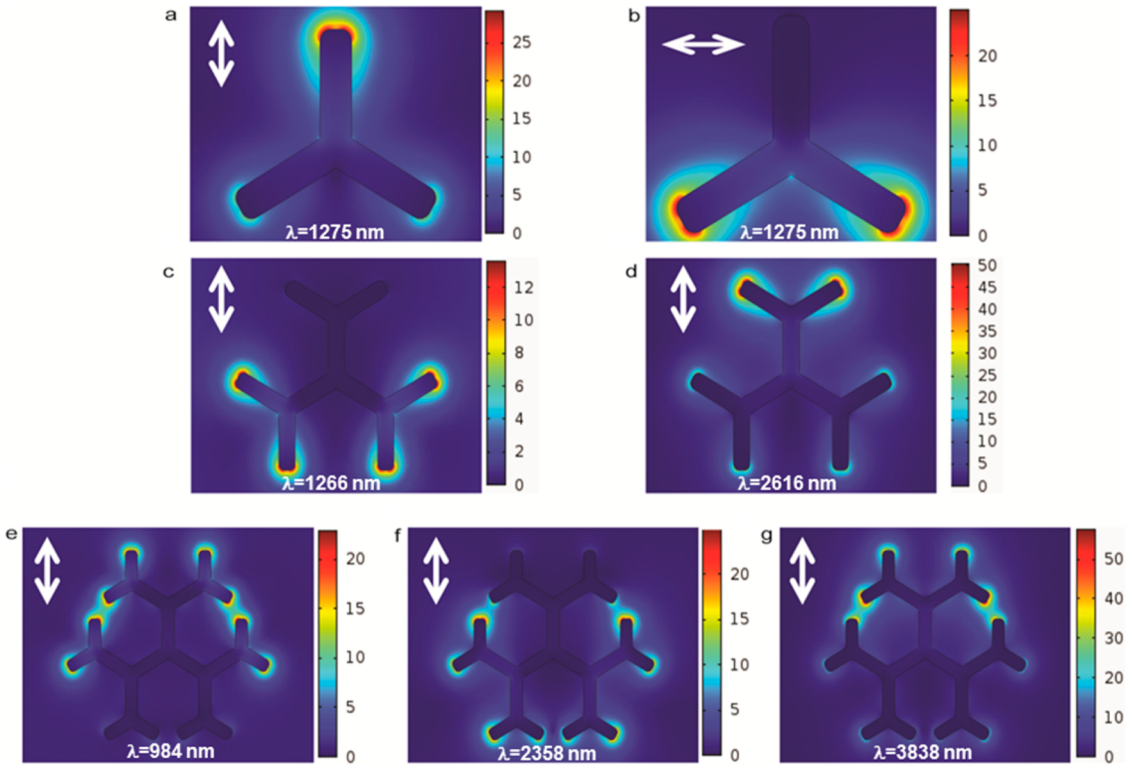

Figure 2. Cayley tree near-field images. FEM simulated near-field plots of the first-order (a,b), second-order (c,d), and third-order structures (e−g). White arrows indicate polarization of excitation. (a) Light (λ = 1275 nm) polarized along the vertical arm in the first-order structure shows E-field concentration most strongly at the end of the vertical arm, with weaker fields concentrated near the branching arms (off polarization axis). (b) Light (λ = 1275 nm) polarized perpendicular to the vertical arm excites E-fields near the ends of the branching arms, with no field concentrated on the vertical arm. (c) At λ = 1266 nm, the higher energy local plasmon is excited with E-fields concentrated locally on the outermost branches. (d) Lower energy global plasmon is excited at λ = 2616 nm. (e) Highest energy third-order structure's plasmon mode (λ = 984 nm). (f) Next highest energy third-order plasmon mode (λ = 2358 nm). (g) Lowest energy global third-order plasmon mode (λ = 3838 nm).

Figure 1d−f. With each iteration of the fractal geometry, N, an N^{th} resonant mode appears at an energy lower than the $(N - 1)^{th}$ resonant mode. For a symmetric N^{th}-order Cayley tree, there are N distinct extinction peaks. Here we observe that, by increasing the fractal order N, the spectral density of the optical resonances at lower energies is increased. One can anticipate from this trend that a dense optical spectrum extending further into the mid- and far-IR would be obtained by additional iterations of the Cayley tree geometry. It is important to note that the additional modes seen with each iteration of the fractal order are not higher-order modes (quadrupole, *etc.*) often seen in nanospheres and nanorods but are all dipolar modes.[26,27] We did not observe the higher-order modes in our experiments mainly because of the detection cutoff region.

The E-field maps corresponding to excitation at each peak resonant wavelength are shown in Figure 2. Figure 2a,b shows the result of vertically and horizontally polarized excitations of the first-order Cayley tree at λ = 1275 nm. These calculations show that under polarized excitation the E-fields are most concentrated at the terminal ends, primarily at the tips of the component arms along the polarization axis in each case. Under horizontal polarization, for example, the field is concentrated primarily at the ends of the arms off the vertical axis. For simplicity, only the fields excited by the vertically polarized E-field are shown and discussed for the higher-order structures. The modes shown in Figure 2c−g are not necessarily single eigenmodes of the structure as the eigenmodes cannot be simply separated by linear E-field polarization in the higher-order structures, which can be understood from the mode degeneracies discussed below. The higher energy resonant mode of the second-order Cayley tree has the strongest E-fields localized at the tips of the outermost arms and virtually no E-field concentrated at the center of the particle. The lower energy resonant mode shows the E-field distributed from the center to the outermost tips (Figure 2d). The third-order structure reveals a similar trend, as the highest energy resonant mode concentrates the energy at the terminal arms (Figure 2e), and each subsequent mode increases the proportion of the field near the center of the particles (Figure 2f,g). Coupling between the outermost arms of different branches may be occurring in the third-order structures (Figure 1g), though the distance between arms of different branches is ∼70 nm. The larger field localization

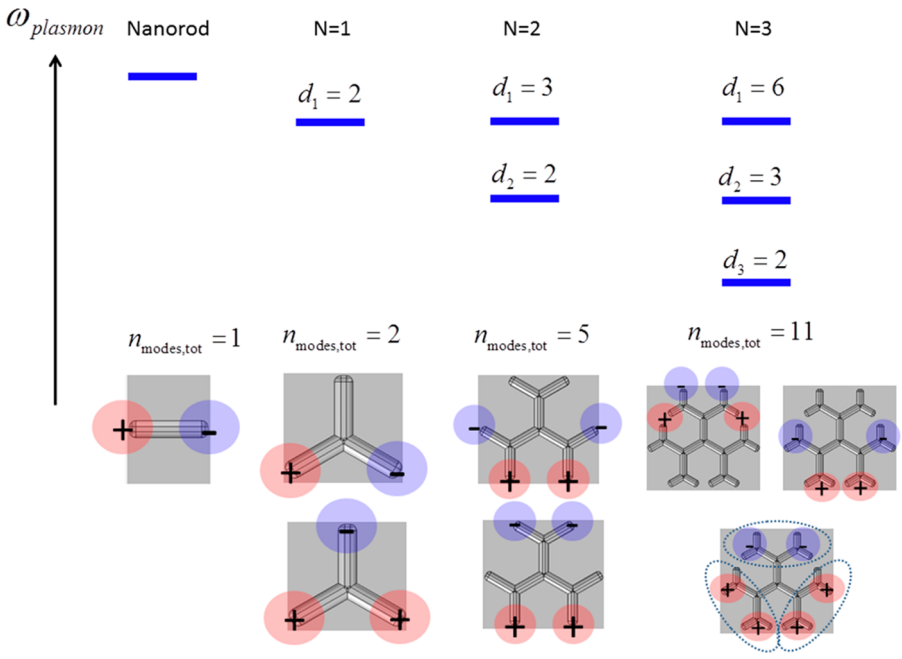

Figure 3. Schematic of formation of the multipeak plasmonic spectra. This principle to generate plasmonic modes is described in the text and is based on the assumption of changes located only on the tips. Mode 1 with the corresponding degeneracy d_1 (N) is the dipolar interarm oscillation of charge. Mode 2 is the interbranch oscillation. Mode 3 on the fractal $N = 3$ is more like a "global" plasmon. In this and other analogous more extended plasmon modes, the charge oscillates between the complex branches shown with dashed ovals (lower right corner of the figure).

in the lowest energy cases (the global plasmons) allows for a broad distribution of the "hot spots", while the higher energy resonances are confined to particular spatial regions. Here one can also see that the outermost tips are broad-band hot spots since they show the largest field strengths at all peak resonances. All simulations were performed on single structures with the same size parameters as the experimental structures in Figure 1.

The number of resonances for fractal order N and their degeneracies can be understood in the following manner. As seen in Figure 2, the induced charges upon plasmon excitation are concentrated at the tips of the structures, while the induced charge density in the center of each structure is always very small. Then, the problem of the plasmonic eigenmodes of a Cayley tree can be approximately reduced to a problem of charges at the vertices of the structure. The charges at the vertices are denoted Q_i, where i is the vertex index. For example, the first-order structure has three tips, $i = 1, 2, 3$. Conservation of charge dictates that $\Sigma_{i=1}^{N_{tips}} Q_i = 0$, where N_{tips} is the number of tips and constrains of the variable Q_i. A tree of order N has $3 \times 2^{N-1}$ tips. Due to charge conservation, only $N_{tips} - 1$ independent variables exist. A set of variables $\{Q_1,Q_2,...Q_{n-1}\}$ gives an eigenvector of the plasmonic mode, and these eigenvectors can be chosen to be orthogonal, as in the quantum mechanical treatment of wave functions (of course, the systems here are purely classical). The total number of longitudinal plasmon eigenmodes is equal to the number of independent variables $N_{tips} - 1$. Another constraint is the three-fold rotational symmetry. For $N = 1$, there exist two modes. For the symmetric $N = 1$, the two orthogonal modes are shown in Figure 2a,b. The two orthogonal eigenmodes can be written as $\{Q_1,Q_2\} = \{1,1\}$ and $\{1,-1\}$, where $\{Q_1,Q_2\}$ are the charges on any two tips of the first-order Cayley tree. Only one mode is observed as the two modes are degenerate due to symmetry. In the same manner, the symmetric second-order structure has five modes, where the higher energy mode is triply degenerate and the lower energy mode is doubly degenerate (Figure 1e). For the symmetric $N = 3$ case, 11 modes exist; however, due to the symmetry, only three resonances appear (Figure 1f). The mode degeneracies are 6, 3, and 2 from high to low energy. In Figure 3, we summarize the principle of formation of the fractal spectrum. With increasing number N, the optical spectrum acquires plasmons with longer wavelengths since the electric current paths for oscillating charges in such plasmons become longer.

In symmetric structures, the resonances are independent of incident polarization. The plasmon resonances excited with orthogonal polarizations of light are equal in energy and line shape but distinct in spatial field enhancement. This degenerate response is not surprising given the C_{3v} symmetry group and can be likened to studies done by Chuntonov *et al.*[28] and Brandl *et al.*[29] on nanoparticle trimers. The Cayley tree geometry itself has D_{3h} symmetry, but with the inclusion of a substrate, the symmetry is reduced to C_{3v}. Through symmetry breaking, the degeneracy of these modes is lifted.

Influence of the Periodic Array Effect and Dielectric Function on Line Width Broadening. We also observed a discrepancy in line shape between the theory and experimental spectra, where the experimental features appeared consistently narrower than the theoretically calculated spectra. While this may initially appear to be nonphysical, it is an important characteristic of how the experimental samples were made. Our fabricated Cayley trees were patterned in periodic arrays with a 500 nm periodicity for the first-order structures and a 1 μm periodicity for the second- and third-order structures. On the other hand, in FEM simulations, only the unit cell of the structure was considered because the periodicity size is large compared with the size of the structures, and the near-field interaction is very small and can be neglected. In our experimental samples, a periodic array effect is present and is responsible for the observed spectral narrowing of the resonant line shape.[30,31] This is examined in more explicit detail in the Supporting Information. In Figure S1a, the spectral response of a small-size first-order Cayley tree is calculated under periodic boundary conditions and compared to the simulated single-particle resonance: the spectral feature is substantially narrower for the periodic case. Interestingly, it was found that the far-field diffractive coupling due to periodicity only affects the line shape of the higher energy plasmon peak and leaves the lower energy plasmon resonance unaffected.

Another factor that can influence broadening is the dielectric function. For plasmonic structures composed of Au, Johnson and Christy[32] as well as Palik[25] data have been widely used. In the current simulations, the Palik data were used because the observed plasmon resonances can appear as low in energy as 0.4 eV, while Johnson and Christy data extend only down to 0.6 eV. In Figure S1b, the first-order structure is simulated using both Johnson and Christy as well as Palik data. We observe that using the Johnson and Christy data results in narrower line shapes in the visible and near-infrared regions, which correspond to the experimental spectrum narrowed by far-field coupling. By employing Palik data, all of the optical features can be simulated, and peak positions agree well with experiments, with the slightly broader spectral line widths that agree with the plasmon line shape of the isolated structure.

Spectral Tunability. The tunability of the spectral response of the first-order structures was studied by symmetrically varying all arm lengths simultaneously and confirmed by simulations of the extinction cross section (Figure 4). All arm lengths were varied from 100 to 180 nm. A red shift of the resonant modes is observed with nonpolarized excitation in all structures as arm lengths are increased, similar to the increasing of the aspect ratio in nanorods[26] or increasing the radius in nanodisks.[4] The peak resonance position

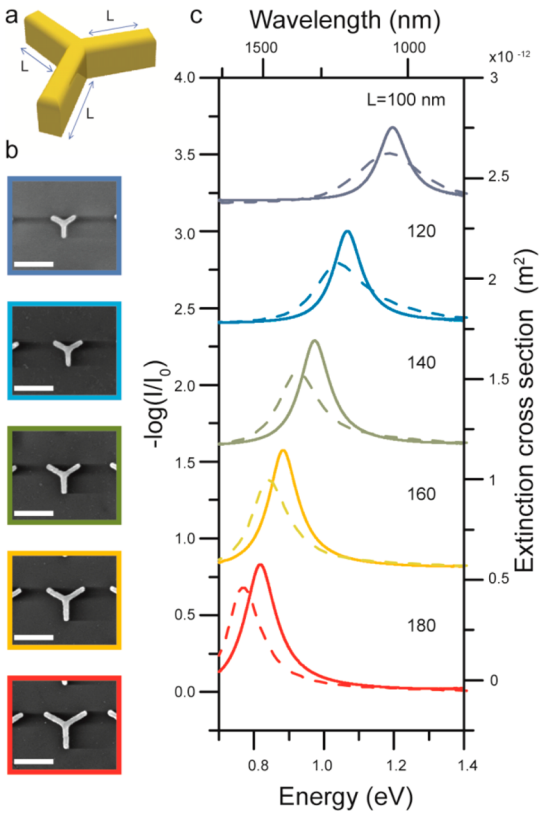

Figure 4. Plasmon tunability of a first-order Cayley tree. (a) All arm lengths *L* are varied symmetrically, while the arm height (50 nm) and arm width (40 nm) are kept constant. (b) SEM images of each symmetric first-order Cayley tree, with arm lengths increased from 100 to 180 nm (top to bottom) in 20 nm increments. The scale bar is 300 nm. (c) Spectra are plotted in absorbance ($-\log[I/I_0]$) (solid lines) along with simulations (dashed lines) of the extinction cross section. With increasing arm length, the maximum resonance position red shifts from 1035 to 1515 nm (1.20 to 0.82 eV).

tunes linearly in wavelength from 1035 to 1515 nm (1.20−0.82 eV), with approximately a 6 nm resonance shift for each nanometer in structure radius.

To systematically investigate the response of the second-order structure, the inner (L_1) and outer (L_2) arms were varied independently and were also varied simultaneously. In all cases, C_{3v} symmetry was maintained. While the inner arm lengths were varied independently of the outer arm lengths from 100 to 180 nm, the higher energy resonant mode remained stationary and the lower energy resonant mode is tuned as a function of inner arm length (Figure 5a). The higher energy resonant mode is therefore independent of inner arm length, which agrees with our understanding of this behavior obtained from the simulated E-field (Figure 2c). When the outer arm lengths are varied independently of the inner arm lengths, both resonant modes are tuned (Figure 5b). The higher energy resonance is confined locally to the outermost branching arms and is sensitive to the outermost arm length, while the lower energy resonance is delocalized over the entire particle (Figure 2d) and

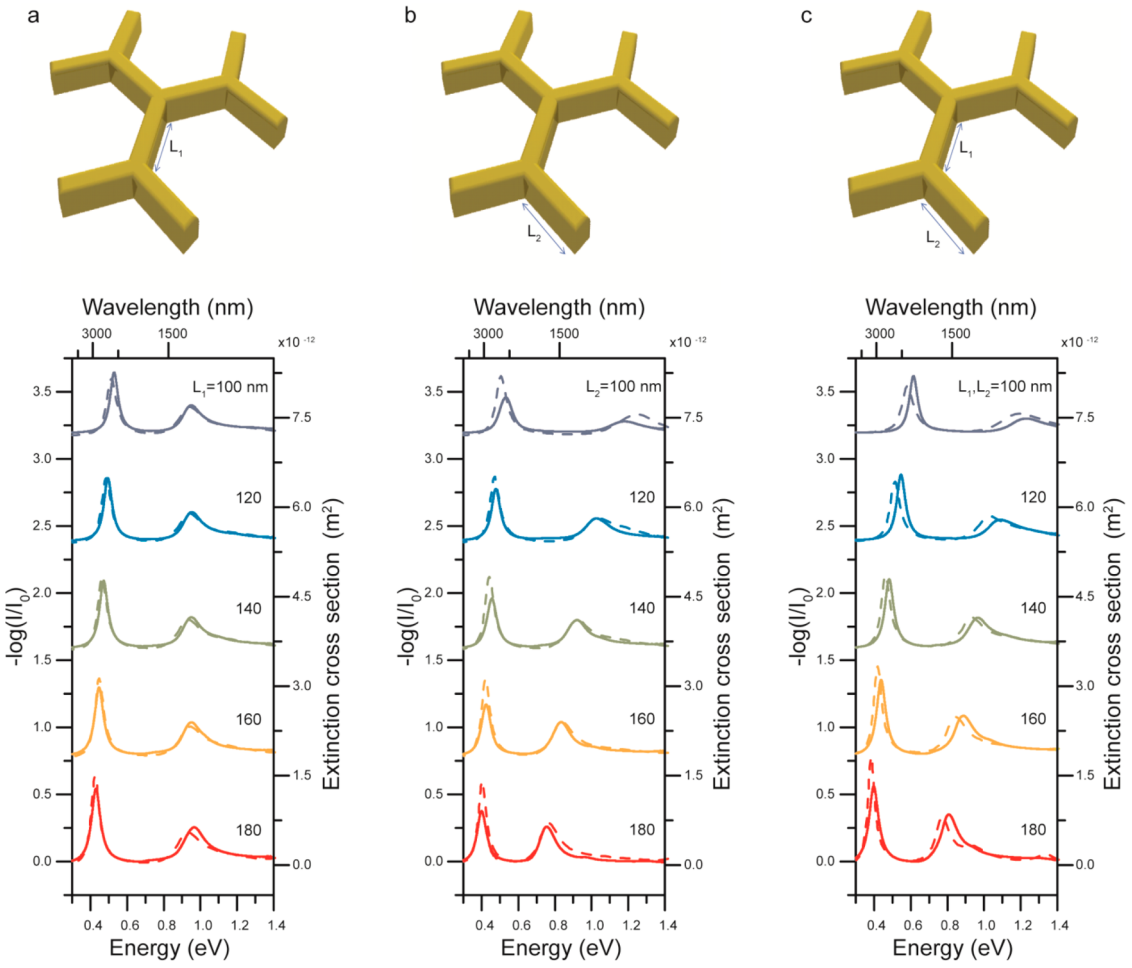

Figure 5. Plasmon tunability of the second-order Cayley tree. (a) As the inner arm lengths (L_1) are increased symmetrically from 100 to 180 nm in 20 nm increments while holding the outer arm lengths (L_2) constant, the lower energy resonance red shifts and the higher energy resonance remains stationary. (b) When the outer arms (L_2) are increased symmetrically and the inner arms remain constant (L_1), both resonances red shift. (c) As the entire structure is increased in size symmetrically (L_1, L_2), both resonances red shift. Spectra are plotted in absorbance ($-\log[I/I_0]$) (solid lines) along with simulations (dashed lines) of the extinction cross section.

depends upon the total structure geometry. When all arm lengths are varied simultaneously, both resonant modes are tuned (Figure 5c). Utilizing this information, we can tune the two resonant modes selectively by choosing an outer arm length and a total structure radius to define the particle's optical response. The spatially and spectrally distinct resonances show no interference in the geometries investigated here, but for certain cases, there could be coupling within individual structures as the spatial and spectral responses could be made to overlap (for example, by reducing the inner arm lengths (L_1) while increasing the outer arm lengths (L_2), the lower energy resonance will blue shift, while the higher energy resonance will red shift, potentially inducing a spectral overlap).

Retardation Effects on Cayley Trees. For small nanorods (ellipsoids), there is a scaling law that the plasmon resonance peak is nearly linearly dependent on the aspect ratio (the ratio of the longer dimension to the shorter dimension). However, such a scaling law can only be applied to small structures: with increasing size, retardation effects begin to dominate, and the scaling law will be gradually destroyed, leaving only a linear behavior between plasmon peak wavelength and a single dimension without regard for aspect ratio. Considering that the arm lengths in each Cayley tree fabricated here are greater than 100 nm, we expect large retardation effects. In Figure S2, the structure ratio (arm length over arm width) is kept constant at 3.5, and no clear scaling law is observed. In the presence of such large retardation effects, it is nearly impossible to observe scaling behavior. However, if we only vary arm length or arm width, the linear dependence of the plasmon peak on structure ratio still survives, as discussed above.

Symmetry Breaking. To aid in our understanding of the broad-band response of fractal particles and films, asymmetries were introduced into the first-order structure. The vertical arm length in the first-order structure was varied from 60 to 260 nm, while the branching

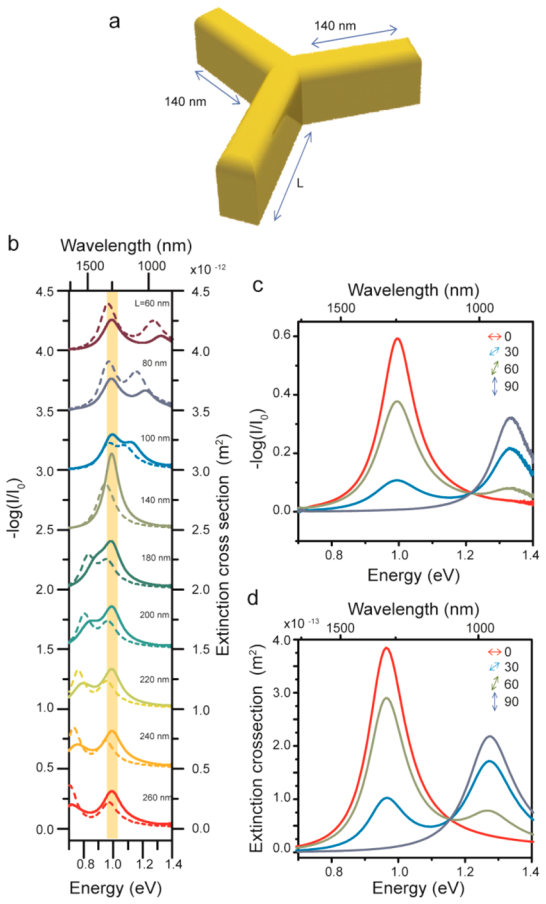

Figure 6. Symmetry breaking introduces polarization dependent modes. (a) To break symmetry in the first-order structure, two arms were kept constant (140 nm), while one arm was increased in length (*L*). (b) As *L* is increased, a resonance is seen to red shift through the spectrum under nonpolarized excitation. These two modes can be excited independently of one another with orthogonal linear polarizations of light (c,d). (c) Experimental polarization dependence for *L* = 60 nm and (d) simulated polarization dependence for *L* = 60 nm. Light polarized at 0° (red curve) excites a mode depending on the branching arm lengths (140 nm), and so a resonance at ∼1 eV is observed in all spectra in (b). The mode excited by light polarized at 90° (dark blue (c,d)) depends on arm length. Incident light polarized off-axis excites a superposition of both modes.

arms were kept constant at 140 nm, reducing the point group symmetry from C_{3v} to C_{2v}. Under nonpolarized light excitation, the spectral response appears to broaden. This broadening is in fact due to the superposition of two polarization-dependent resonances, as the degeneracy of the C_3 rotational symmetry is lifted. Each structure was excited by light linearly polarized at 0, 30, 60, 90, 120, 150, and 180°. For each structure excited by light polarized perpendicular to the vertical axis (0°), a resonance is seen at ∼1.0 eV (Figure 6), corresponding to the excitation of the off-axis branched mode (Figure 2b). Light polarized parallel to the vertical axis (90°) excites a resonance dependent on the asymmetric arm length (Figure 6). Light polarized off-axis (30 or 60°) couples into these two distinct modes in relation to decomposing the light into

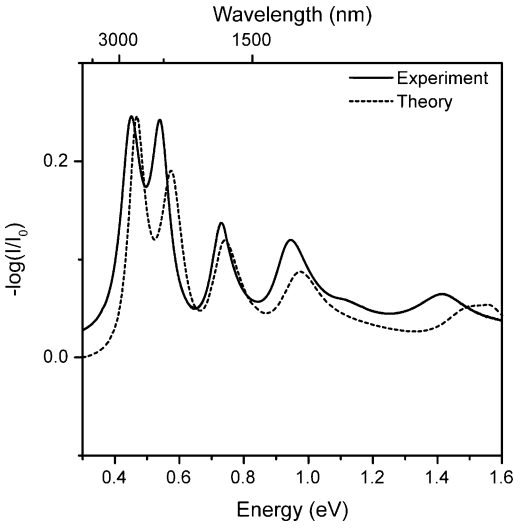

Figure 7. Experimental (solid) and simulated (dashed) spectra for a second-order Cayley tree with three different pairs of outer arms (80, 140, and 200 nm), with inner arms of 140 nm. The five modes of this structure can be easily distinguished from one another and span from the visible into the mid-infrared. The simulation result has been normalized to the experimental result.

component vectors along these axes (Figure 6c,d). In the symmetric case, both modes are degenerate, while in the asymmetric case, the two modes can be tuned independently. The vertical arm mode was red-shifted as the arm length was increased from 60 to 260 nm. The two resonances do not interfere with one another because they are spatially isolated and, therefore, do not give rise to coherent effects. In extreme cases, a semitransparent window was created by increasing the distance between the spectral positions of the two resonances (Figure 6b). A further reduction of symmetry, C_1, was investigated by varying all arm lengths independently, revealing again two polarization-dependent modes.

To further demonstrate the separation of modes with increasing asymmetry, the second-order Cayley tree was fabricated with symmetric inner arms, L_1, of 140 nm but with three different pairs of outer arms, L_2, of 80, 140, and 200 nm (Figure 7). The low energy modes can be understood as global resonances and are analogous to the coupled arms in the first-order structure. The three higher energy modes come from the intrabranch interactions of the outer arms, and so it is simple to see why three modes exist in this case. Moreover, this structure has five distinct resonances spanning from the visible into the mid-infrared.

Additional symmetry breaking could be introduced by changing the vertex angle, creating a distinct C_{2v} symmetry. In this symmetry-broken geometry, it is likely that there would be the introduction of polarization-dependent resonances as well as spectral shifts, similar to the case discussed by Chuntonov *et al.*[28]

Advantage of the Cayley Tree Geometry. Alternatively to a fractal approach, a similar spectral response could be

engineered using a collection of nanorods of various lengths corresponding to each spectral position. The disadvantages of such a geometry is that all "hot spots" are located at the ends of the nanorods and a variety of structures would be required. We have demonstrated here a series of simple single structures with multiple resonances spanning from the near to mid-IR confined in single hot spots. The spatial field distributions investigated here are dependent on the geometry as well as the wavelength.

Additionally, the extinction of the Cayley tree is compared theoretically to nanorod and nanodisk geometries. In Figure S3, we show the extinction spectra for three shapes under two polarizations: fractal, nanorod, and V-shape fractal. One can see that fractal trees with C_3 symmetry are isotropic, and if we define extinction efficiency as $\beta_{ext} = \sigma_{extinct\ \ cross\ \ section}/\sigma_{physical\ \ cross\ \ section}$, then under nonpolarized light, Cayley trees would obviously provide larger extinction efficiency than the other structures, as shown in Figure S3d. For other isotropic shapes like a disk, for example, the comparison is shown in Figure S4, where the enhancement of extinction efficiency is much larger. Thus, the Cayley trees will be a very promising structure in future engineering and design of optical sensors.

In this study, the tips of fractal trees were designed to have flat edges but not sharp edges, as shown in Figure S5a. There is no doubt that sharp edges would generate a larger field enhancement around tips, but as shown in Figure S5b,c, the peak extinction enhancement and field enhancement show only a very small improvement for the sharp-tip case. If we define an effective hot spot area as the total surface area with field enhancement larger than 80% of the maximum field enhancement, then the effective hot spot area is 7.34 nm^2 for the flat edge case and 1.13 nm^2 for the sharp edge case (Figure S5). We could anticipate that this geometry could be very useful and practical for biological and chemical-sensing applications.

We hypothesize that the properties of branched structures at the onset of self-similarity, which we have described here, may also be applicable to similar branching self-similar geometries beyond the Cayley tree, such as additional binary, tertiary, and random fractal systems. Extending this initial study may reveal that certain fractal geometries may be optimal for applications such as biological and chemical sensing, while others may be better suited for enhancing nonlinear optics, for example, for higher harmonic generation, depending on their resonant wavelengths and spatial location of enhanced fields.

CONCLUSION

We have demonstrated a novel multiresonant plasmonic nanoantenna system with resonances spanning the near- to mid-IR. The *N*th-order symmetric (C_{3v}) Cayley tree system contains *N* peaks in the extinction spectra. By increasing the arm lengths in the symmetric structures, all resonances are seen to red shift. In the second-order structures, the higher energy (local) resonance is a function of the outer arm length, while the lower energy (global) resonance is a function of total structure geometry. Mode-selective excitation with polarized light occurs in first-order Cayley tree structures with reduced symmetry (C_{2v} and C_1). In summary, we have demonstrated that an *N*th-order Cayley tree will have *N* tunable resonant modes that can be polarization-dependent in reduced symmetry geometries. Using this or other fractal geometries, plasmonic particles may provide a promising geometry that can be engineered for uses in chemical analysis as well as nonlinear optics. Nanostructures with these optical properties also open up the possibility of new media or materials with engineered transparency windows.

MATERIALS AND METHODS

Cayley Tree Fabrication. High-grade quartz substrates (Infrasil 302, Heraeus Optics) were sonicated in acetone for 5 min, rinsed with isopropyl alcohol (IPA), and coated with a 200 nm thick layer of poly(methyl methacrylate) A4 950 resist (MicroChem), followed by a 20 nm thick layer of ESPACER (Showa Denko). Following e-beam exposure and development (water to remove Espacer, and 3:1 IPA/MIBK), a 2 nm pure Ti (Kamis) adhesion layer was deposited prior to a 50 nm pure Au (Kamis) layer using electron-beam evaporation at a rate of ~1 A/s for both metals. The liftoff was performed in N-methyl-2-pyrrolidine at 65 °C, followed by an IPA rinse. Each array was fabricated with an area of 50 × 50 μm^2, and electron micrographs of each structure were obtained (FEI Quanta 600).

Fourier Transform Infrared Spectroscopy. The optical transmission measurements were made by an FTIR spectrometer (Bruker Vertex 80v FTIR, tungsten and globar light sources) equipped with a microscope (Hyperion 3000, 36× Schwarzchild objective, NA = 0.5, liquid-nitrogen-cooled MCT, and InGaAs single element detectors). A quartz linear polarizer was placed in the excitation pathway for the polarization-dependent measurements.

Theoretical Calculations. Modeling was performed using the finite element method (COMSOL) with Cayley trees defined by arm lengths specified in the text, arm widths of 40 nm, a thickness of 50 nm, and a 10 nm radius of curvature for the upper edges. The extinction cross section was calculated using the Palik dielectric values for gold.[25] The structures were placed on a finite substrate of quartz (ε = 2.4) of 300 nm thickness. In the next step, the extinctions of a single structure were calculated and then the contribution from the bare substrate was subtracted.

Conflict of Interest: The authors declare no competing financial interest.

Acknowledgment. We gratefully acknowledge the funding and support provided by Welch Foundation Grant C-1222 and Army Research Office MURI W911NF-12-1-0407.

Supporting Information Available: Comparison of periodic array resonances to that of single structures and the effect of

Johnson and Christy *vs* Palik dielectric data on line shape in Figure S1. Extinction spectra of the first-order structure with fixed aspect ratio reveal that there is no simple scaling law as seen in Figure S2. Extinction spectra under two polarizations for the first-order Cayley tree, a nanorod, and a V-shape comparing the extinction efficiency of the three structures in Figure S3. Figure S4 compares the extinction efficiency of the first-order Cayley tree with nanodisks of the same radius of the Cayley tree and of the same physical cross section. Figure S5 compares field enhancements of the first-order Cayley tree structure with sharp edges to the same structure with flat edges. This material is available free of charge *via* the Internet at http://pubs.acs.org.

REFERENCES AND NOTES

1. Kneipp, J.; Kneipp, H.; Kneipp, K. SERS—A Single-Molecule and Nanoscale Tool for Bioanalytics. *Chem. Soc. Rev.* **2008**, *37*, 1052–1060.
2. Brown, L. V.; Zhao, K.; King, N.; Sobhani, H.; Nordlander, P.; Halas, N. J. Surface-Enhanced Infrared Absorption Using Individual Cross Antennas Tailored to Chemical Moieties. *J. Am. Chem. Soc.* **2013**, *135*, 3688–3695.
3. Navarro-Cia, M.; Maier, S. A. Broad-Band Near-Infrared Plasmonic Nanoantennas for Higher Harmonic Generation. *ACS Nano* **2012**, *6*, 3537–3544.
4. Knight, M. W.; King, N. S.; Liu, L.; Everitt, H. O.; Nordlander, P.; Halas, N. J. Aluminum for Plasmonics. *ACS Nano* **2014**, *8*, 834–840.
5. Kimling, J.; Maier, M.; Okenve, B.; Kotaidis, V.; Ballot, H.; Plech, A. Turkevich Method for Gold Nanoparticle Synthesis Revisited. *J. Phys. Chem. B* **2006**, *110*, 15700–15707.
6. Oldenburg, S.; Averitt, R.; Westcott, S.; Halas, N. J. Nanoengineering of Optical Resonances. *Chem. Phys. Lett.* **1998**, *288*, 243–247.
7. Bardhan, R.; Mukherjee, S.; Mirin, N. A.; Levit, S. D.; Nordlander, P.; Halas, N. J. Nanosphere-in-a-Nanoshell: A Simple Nanomatryushka. *J. Phys. Chem. C* **2010**, *114*, 7378–7383.
8. Millstone, J. E.; Hurst, S. J.; Métraux, G. S.; Cutler, J. I.; Mirkin, C. A. Colloidal Gold and Silver Triangular Nanoprisms. *Small* **2009**, *5*, 646–664.
9. Perezjuste, J.; Pastorizasantos, I.; Lizmarzan, L.; Mulvaney, P. Gold Nanorods: Synthesis, Characterization and Applications. *Coord. Chem. Rev.* **2005**, *249*, 1870–1901.
10. Anderson, L. J. E.; Payne, C. M.; Zhen, Y.-R.; Nordlander, P.; Hafner, J. H. A Tunable Plasmon Resonance in Gold Nanobelts. *Nano Lett.* **2011**, *11*, 5034–5037.
11. Nehl, C. L.; Liao, H.; Hafner, J. H. Optical Properties of Star-Shaped Gold Nanoparticles. *Nano Lett.* **2006**, *6*, 683–688.
12. Van Duyne, R. P.; Hulteen, J. C.; Treichelb, D. A. Atomic Force Microscopy and Surface-Enhanced Raman Spectroscopy. I. Ag Island Films and Ag Film over Polymer Nanosphere Surfaces Supported on Glass. *J. Chem. Phys.* **1993**, *99*, 2101–2115.
13. Yue, W.; Wang, Z.; Yang, Y.; Chen, L.; Syed, A.; Wong, K.; Wang, X. Electron-Beam Lithography of Gold Nanostructures for Surface-Enhanced Raman Scattering. *J. Micromech. Microeng.* **2012**, *22*, 125007.
14. Baliarda, C. P.; Romeu, J.; Cardama, A. The Koch Monopole: A Small Fractal Antenna. *IEEE Trans. Antennas Propag.* **2000**, *48*, 1773–1781.
15. Dong, J.; Qu, S.; Zheng, H.; Zhang, Z.; Li, J.; Huo, Y.; Li, G. Simultaneous SEF and SERRS from Silver Fractal-like Nanostructure. *Sens. Actuators, B* **2014**, *191*, 595–599.
16. Hou, C.; Meng, G.; Huang, Q.; Zhu, C.; Huang, Z.; Chen, B.; Sun, K. Ag-Nanoparticle-Decorated Au-Fractal Patterns on Bowl-like-Dimple Arrays on Al Foil as an Effective SERS Substrate for the Rapid Detection of PCBs. *Chem. Commun.* **2014**, *50*, 569–571.
17. Stockman, M. I.; Shalaev, V. M.; Moskovits, M.; Botet, R.; George, T. F. Enhanced Raman Scattering by Fractal Clusters: Scale-Invariant Theory. *Phys. Rev. B* **1992**, *46*, 2821–2830.
18. Tsai, D. P.; Kovacs, J.; Wang, Z.; Moskovits, M.; Shalaev, V. M.; Suh, J. S.; Botet, R. Photon Scanning Tunneling Microscopy Images of Optical Excitations of Fractal Metal Colloid Clusters. *Phys. Rev. Lett.* **1994**, *72*, 4149–4152.
19. Volpe, G.; Quidant, R. Fractal Plasmonics: Subdiffraction Focusing and Broadband Spectral Response by a Sierpinski Nanocarpet. *Opt. Express* **2011**, *19*, 3612–3618.
20. Zhou, L.; Chan, C. T.; Sheng, P. Theoretical Studies on the Transmission and Reflection Properties of Metallic Planar Fractals. *J. Phys. D: Appl. Phys.* **2004**, *37*, 368–373.
21. Wen, W.; Zhou, L.; Li, J.; Ge, W.; Chan, C. T.; Sheng, P. Subwavelength Photonic Band Gaps from Planar Fractals. *Phys. Rev. Lett.* **2002**, *89*, 223901.
22. Aouani, H.; Rahmani, M.; Šípová, H.; Torres, V.; Hegnerová, K.; Beruete, M.; Homola, J.; Hong, M.; Navarro-Cía, M.; Maier, S. A. Plasmonic Nanoantennas for Multispectral Surface-Enhanced Spectroscopies. *J. Phys. Chem. C* **2013**, *117*, 18620–18626.
23. Li, K.; Stockman, M. I.; Bergman, D. J. Self-Similar Chain of Metal Nanospheres as an Efficient Nanolens. *Phys. Rev. Lett.* **2003**, *91*, 227402.
24. Thyagarajan, K.; Rivier, S.; Lovera, A.; Martin, O. J. F. Enhanced Second-Harmonic Generation from Double Resonant Plasmonic Antennae. *Opt. Express* **2012**, *20*, 12860–12865.
25. Palik, E. D. Handbook of Optical Constants. *Proc. Natl. Acad. Sci. U.S.A.* **1991**, *2*, 1096.
26. Link, S.; El-Sayed, M. Spectral Properties and Relaxation Dynamics of Surface Plasmon Electronic Oscillations in Gold and Silver Nanodots and Nanorods. *J. Phys. Chem. B* **1999**, *103*, 8410–8426.
27. Zhang, H.; Demir, H.; Govorov, A. Plasmonic Metamaterials and Nanocomposites with the Narrow Transparency Window Effect in Broad Extinction Spectra. *ACS Photonics* **2014**, *1*, 822–832.
28. Chuntonov, L.; Haran, G. Trimeric Plasmonic Molecules: The Role of Symmetry. *Nano Lett.* **2011**, *11*, 2440–2445.
29. Brandl, D. W.; Mirin, N. A.; Nordlander, P. Plasmon Modes of Nanosphere Trimers and Quadrumers. *J. Phys. Chem. B* **2006**, *110*, 12302–12310.
30. Olson, J.; Manjavacas, A.; Liu, L.; Chang, W.-S.; Foerster, B.; King, N. S.; Knight, M. W.; Nordlander, P.; Halas, N. J.; Link, S. Vivid, Full-Color Aluminum Plasmonic Pixels. *Proc. Natl. Acad. Sci. U.S.A.* **2014**, *111*, 14348–14353.
31. Zhao, L. L.; Kelly, K. L. K.; Schatz, G. C. The Extinction Spectra of Silver Nanoparticle Arrays: Influence of Array Structure on Plasmon Resonance Wavelength and Width. *J. Phys. Chem. B* **2003**, *107*, 7343–7350.
32. Johnson, P.; Christy, R. Optical Constants of the Noble Metals. *Phys. Rev. B* **1972**, *6*, 4370–4379.